The Effect of Thermal Cycling on the Fracture Toughness of Metallic Glasses

Jittisa Ketkaew[1], Rui Yamada[2], Hui Wang[3], Derek Kuldinow[1], Benjamin Sol Schroers[1], Wojciech Dmowski[3], Takeshi Egami[3, 4], Jan Schroers[1]

[1] *Department of Mechanical Engineering & Materials Science, Yale University, New Haven, CT 06511, USA*
[2] *Frontier Research Institute of Interdisciplinary Science (FRIS), Tohoku University, Sendai, 980-8578, Japan*
[3] *Department of Materials Science and Engineering, University of Tennessee, Knoxville, TN 37996, USA*
[4] *Oak Ridge National Laboratory, Oak Ridge, TN 37831, USA*

Abstract

A wide range of behaviors, including non-monotonic rejuvenation and relaxation, and the ability to qualitatively change the effect by varying the structural state of the glass was observed during thermal cycling of bulk metallic glasses. For this, we considered various bulk metallic glasses, $Zr_{44}Ti_{11}Cu_{10}Ni_{10}Be_{25}$, $Pd_{43}Cu_{27}Ni_{10}P_{20}$, $Pt_{57.5}Cu_{14.7}Ni_{5.3}P_{22.5}$, and $La_{55}Al_{25}Ni_{20}$, at various fictive temperatures to study the effect of thermal cycling on structure, thermal signature, and fracture toughness. For some BMGs and conditions considered here, thermal cycling results in a looser structure and an increase in fracture toughness. We found that for certain other BMGs and conditions, thermal cycling results in relaxation, reflected in a denser structure, and a decrease in fracture toughness. All these responses are non-monotonic and reveal a pronounced extremum with fracture toughness values of ± 50% of the original value, before approaching a value similar to the original value prior to thermal cycling. Such richness in response to thermal cycling suggests incompleteness of the previous picture where monotonically decreasing local stresses resulting in a homogenization of the structure with increasing cycle number. Our finding suggests that relative comparisons of various contributions including activation barriers for α-relaxation have to be considered which are also constantly changing, to decide if further cycling results in an increase

or a decrease in fracture toughness. The fracture toughness' response to thermal cycling can be correlated with the average atomic structures' response to thermal cycling, while the thermal response does not exhibit an obvious correlation.

Keywords: Bulk metallic glasses; thermal cycling, rejuvenation; structural relaxation; fracture toughness

1. Introduction

Glasses are non-equilibrium materials with a disordered atomic structure that defines their properties. The glasses' structural state is quantified by their fictive temperature (T_f), the temperature at which the supercooled liquid and freezes into a glass [1, 2]. Thereby, at T_f, glass and supercooled liquid are thermodynamically and structurally identical. Strictly speaking, as metallic glasses exhibit typically a heterogeneous structure, a spectrum of fictive temperatures are present. Fictive temperatures have been manipulated through the cooling rate [3], thermal relaxation or annealing [4, 5], ion irradiation [6-9], severe plastic deformation [10, 11], cold rolling [12], high-pressure torsion, and mechanical loadings [13, 14]. Glasses with high energy state or high T_f possess a loosely packed structure and high ductility, while glasses with low energy state or T_f are more densely packed and behaves more brittle (Fig. 1 (a)). Rejuvenation results into a higher T_f state, resulting in increased ductility, while the opposite phenomenon, relaxation results in a more densely-packed structure and a more brittle glass (Fig. 1(b)) [15]. Figure 1(c) summarizes the effects of common methods to manipulate the glasses structure and the associated dominant effects on the glasses structural and energetical state. Recently, thermal cycling was suggested as a tool to rejuvenate metallic glasses whereby the structure would evolve towards one with a higher

T_f [16, 17]. Such rejuvenation has been reported to lead to higher potential energy, improvements in plasticity, ductility, a decrease in hardness, ability to at least partially reverse annealing, and a reduction in compressive strength [16-20]. Technologically, thermal cycling is highly attractive as it offers an opportunity for a scalable and cost-effective technology to enhance some mechanical properties of bulk metallic glasses (BMGs). The effect of thermal cycling on BMG properties has been quantified through compression and bending tests [13, 16, 18, 21-23]. However, a more sensitive macroscopic quantity to structural changes of BMGs is the fracture toughness [24-27] which we propose here as a measure to quantify and gain insights into the mechanisms for thermal cycling for BMGs. Within this work, we consider various BMGs at various T_f's to study the effect of thermal cycling on the glasses' structure, thermal signature, and fracture toughness (K_Q). The results allow us to i) reveal the effect of thermal cycling on the atomic structure, thermal signature, and K_Q ii) determine if the observed behaviors are ubiquitous among BMGs, and iii) determine if and which specific thermal cycling conditions cause rejuvenation or relaxation. We found that i) thermal cycling induces changes in the BMGs' atomic structure, hence, results in a change of K_Q ii) the response to thermal cycling is BMG specific iii) thermal signature and thermal cycling does not have a definite direction, it can result in both rejuvenation and relaxation. Most surprisingly, we found that the effect of thermal cycling is non-monotonic; thermal cycling drives the glass initially further away from (meta) stable equilibrium, which upon further cycling is approached again.

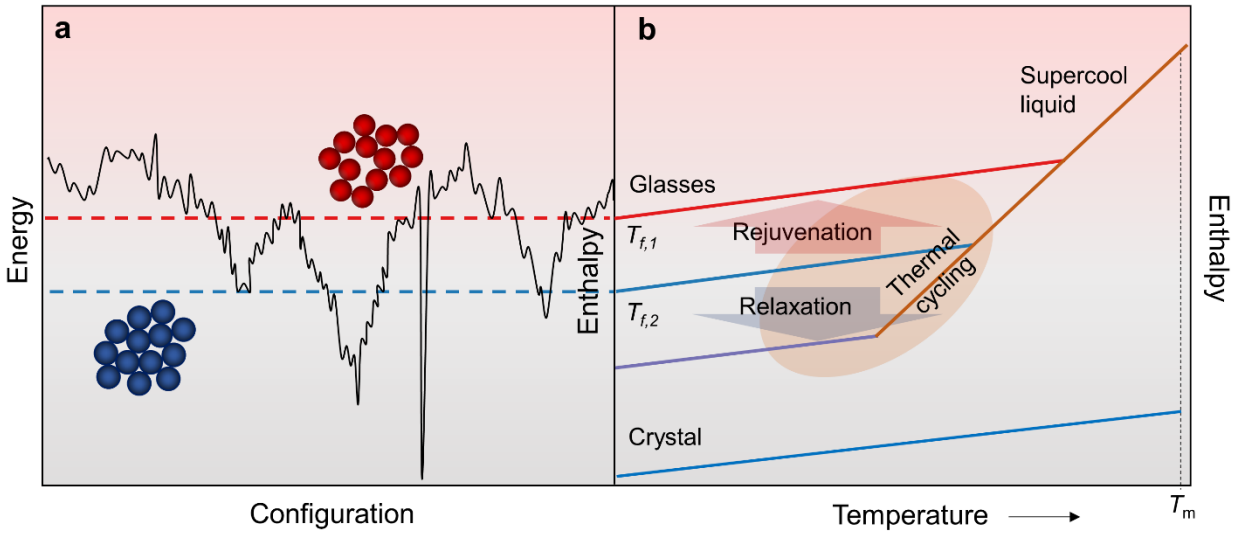

Methods	Dominating effect
Thermal annealing	Relaxation
Fast cooling rate	Rejuvenation
Severe plastic deformation, cold rolling, high pressure torsion, shot peening, neutron scattering	Rejuvenation
Thermal cycling	Rejuvenation
Mechanical static loading	Rejuvenation & relaxation

Fig. 1 (a) The potential energy landscape (PEL) showing various possible states of a glass (b) thermodynamic picture of glasses with various T_f and the effect of relaxation and rejuvenation on the thermodynamic states (here, enthalpy). (c) Summary of common methods to alter the state of the glass.

2. Experimental

2.1 Materials Preparation

To study the effect of thermal cycling on structure, thermal properties, and fracture toughness, we consider $Zr_{44}Ti_{11}Cu_{10}Ni_{10}Be_{25}$, $Pd_{43}Cu_{27}Ni_{10}P_{20}$, $Pt_{57.5}Cu_{14.7}Ni_{5.3}P_{22.5}$, and $La_{55}Al_{25}Ni_{20}$ alloys. The experiments with the considered alloys allow us to draw some general conclusions as the considered alloys exhibit differences in fragility [28], fracture toughness [29], transition metal vs.

transition metal-metalloid based BMGs [30], and cooling rate dependence of their fracture toughness [31]. Fully amorphous samples are fabricated through arc-melting paired with suction-casting and quartz-tube water quenching. Their amorphous structures were verified by X-ray diffraction (Rigaku Smartlab X-ray diffraction) and thermal analysis using a Perkin Elmer Diamond differential scanning calorimetry (DSC). Standard heating with 20 K/min was performed on all as-cast and processed BMGs to evaluate for glass transition temperature (T_g), crystallization temperature (T_x), structural relaxation, and heat of crystallization to confirm the amorphous state and consistency of the fabricated alloy.

2.2 Fracture toughness sample preparation and measurements

Fracture toughness test samples were fabricated through a thermoplastic forming (TPF) method where the BMGs are molded into a silicon mold [32-34]. Resulting BMG test samples are single edge notched tension (SENT) samples with a geometry of 25x5x0.3 mm, notch length of 2.5 mm (a/W=0.5), and notch root radius of ρ = 10 μm. For the BMGs considered in this study, the notch radius of 10 μm is well below the critical notch radius, and thus results in the same K_Q as for an infinitely sharp notch radius [35]. Fabrication of various BMGs in silicon molds is carried out through TPF under a pressure of 20 MPa for 100 s at 703 K, 633 K, and 543 K for Zr-BMG, Pd-BMG and Pt-BMG, respectively, followed by water quenching. This procedure results in uniform and fully amorphous test samples. BMG test specimen were released from silicon molds by etching in 20% KOH solution. Samples were polished to 1 μm finish to ensure uniform surface roughness. We create glasses with specific T_f's by equilibrating the glass at the desired T_f and remain at that temperature until the required relaxation time for the given temperature as suggested by the Vogel-Fulcher-Tammann (VFT) relation [36, 37], is exceeded. Subsequent water quenching ensures that the glass maintains its T_f as long as the respective relaxation time is larger than 0.1 sec [25].

Mechanical testing of as-fabricated fully amorphous BMG with the specified T_f in the shape of SENT samples was performed through uniaxial tensile testing under quasi-static displacement control with an initial strain rate of $10^{-4}s^{-1}$ as described in [38]. At least three samples were fabricated and characterized and reported values are mean values with errors originating from one sigma standard deviation.

The visible shear band propagation ahead of the notch tip were recorded with a CCD camera. The number of shear bands ahead of the notch tip were estimated by counting the visible primary and secondary shear band which is plotted against K_Q and fitted by the power law following the method described in [39]. Fractured surfaces of tested fracture toughness samples were observed under the scanning electron microscope.

2.3 Thermal cycling

Thermal cycling of as-prepared fracture toughness samples and as-cast $La_{55}Al_{25}Ni_{20}$ was carried out in a custom built and fully automated setup with a minimum temperature of 77 K, achieved through liquid nitrogen, and a maximum temperature of 300 K (room temperature). The samples were subjected through various cycles of liquid nitrogen for 60 seconds and room temperature water for 60 seconds. The temperature of the liquid nitrogen and water is monitored by thermocouples. The water was kept at room temperature by heating with a hot plate. Additional experiments were also performed to achieve a different temperature amplitude. Fracture toughness samples were cycled in the same manner as described above between the room temperature and acetone/dry ice solution to achieve temperature between 298 K and 195 K. Summary of all studied conditions are summarized in Table 1, which includes alloy composition, fictive temperatures, and the number of thermal cycles performed.

Alloy	Fictive temperature	Number of thermal cycles
$Zr_{44}Ti_{11}Cu_{10}Ni_{10}Be_{25}$	683 K	0, 50, 200, 300, 400, 500, 700
	603 K, 593 K	0, 200
$Pd_{43}Cu_{27}Ni_{10}P_{20}$	633 K	0, 10, 60, 200, 300, 500
	573 K	0, 50, 200
$Pt_{57.5}Cu_{14.7}Ni_{5.3}P_{22.5}$	543 K	0, 200
$La_{55}Al_{25}Ni_{20}$	As-cast	0, 15

Table 1. Summary of alloys, fictive temperature, and tested number of thermal cycles used in this study.

2.4 Atomic structure and thermal characterization

For all thermally cycled samples, the enthalpy of relaxation (ΔH_{rel}) and heat capacity (C_p) were measured as a function of temperature to evaluate the degree of rejuvenation. The sample was equilibrated at 313 K and then heated to above T_g at a heating rate of 20 K/min and subsequently cooled to 313 K with 20 K/min. The procedure was performed twice. Sapphire samples were used as a reference for C_p measurement. All DSC experiments were performed under argon atmosphere. High-energy X-ray diffraction for characterization of atomic structure was carried out at the Advanced Photon Source (Argonne National Laboratory) beamline 1-ID. The incident energy was tuned to 100 keV and a 2D area detector was placed ~44 cm behind the sample. Calibration was performed using the CeO2 NIST powder standard. High-energy X-ray diffraction data were processed by FIT2D software [40].

The samples were thin plates of thickness ~0.3mm, 5mm in width and 10mm in length. The beam size was 0.2 mm by 0.2 mm. The diffraction geometry is transmission, so the volume of the material under the high energy X-ray beam are 0.2 by 0.2 by the thickness of the sample.

3. Results and discussions

3.1 The effect of thermal cycling on the fracture toughness

For $Pd_{43}Cu_{27}Ni_{10}P_{20}$ and $Zr_{44}Ti_{11}Cu_{10}Ni_{10}Be_{25}$, test samples were fabricated with various T_f's [25]. Figure 2(a) shows K_Q of the Pd-BMG with two different T_f's as a function of number of cycles. The K_Q of the Pd-BMG with a T_f of 633K is measured to be 38.0 ± 1.0 MPa·m$^{1/2}$ in its as-prepared state. Upon thermal cycling, K_Q increases by 45% to a maximum value of K_Q = 56±5 MPa·m$^{1/2}$ at ~200 cycles. This increase in K_Q is consistent with previously reported work on different metallic glasses showing an increase in plastic strain in compression, which was explained by thermal cycling causing rejuvenation of the glass [41]. However, we observed that further thermal cycling results in a lowering of K_Q from its maximum level. Specifically, cycling to ~300 cycles reduce K_Q to 39 ± 5 MPa·m$^{1/2}$, which is comparable to its original value. Even more surprising, Pd-BMG with T_f = 573K and a K_Q of 25 ± 6 MPa·m$^{1/2}$ follows a complete opposite behavior. Initially, with increasing cycling, K_Q drops to 12.1 ± 0.3 MPa·m$^{1/2}$ after 50 cycles. Further cycling up to 200 cycles results in an increase to 22 ± 1 MPa·m$^{1/2}$. Such behavior is in contrast to previously reported effects of thermal cycling on mechanical properties of BMGs [16]. Following such surprising results, the Zr-BMG with a T_f of 683 K exhibits a reduction in K_Q after 200 cycles by ~50% of the original K_Q, shown in Fig. 2(b). Subsequently, with further cycling of up to 700 cycles, the K_Q increases to values similar to its original value. A qualitatively similar behavior to Pd-BMG with

T_f of 573 K is also present in Zr-BMG with T_f of 683 K (Fig 2b). Furthermore, we found that $Pt_{57.5}Cu_{14.7}Ni_{5.3}P_{22.5}$ with T_f = 543 K shows similar response to thermal cycling with the Zr-BMG, after 200 cycles, its K_Q decreased from 88 ± 3 MPa·m$^{1/2}$ to 60 ± 2 MPa·m$^{1/2}$.

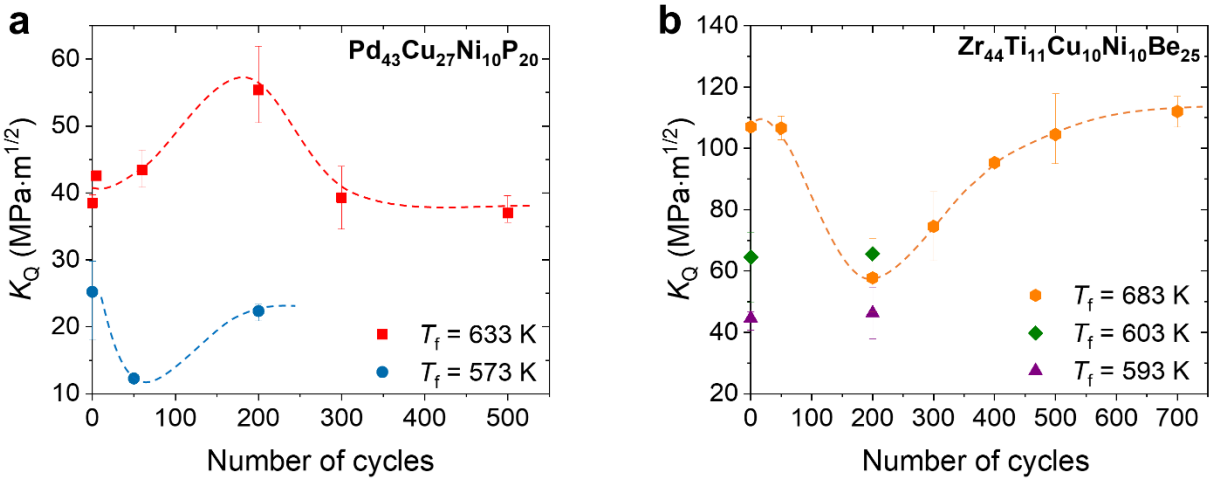

Fig. 2 The effect of thermal cycling (between 70 K and 300 K with 60 sec holding time) on the fracture toughness, K_Q, of (a) Pd-BMG and (b) Zr-BMG with various fictive temperatures.

Figure 3(a) shows representative plastic zone regions in front of the notch before fracturing for Pd- and Zr-BMG corresponding to fracture toughness data in Fig.2. It should be mentioned that the plastic zone size, the region in which plastic work is carried out to contribute to the fracture toughness may exceed significantly beyond the visible zone which is characterized here [42, 43]. The visible final plastic zone size on the surface, R_p, for Pd-BMG with T_f = 633 K without thermal cycling is ~56 μm and is largest at 200 cycles of 107 μm, then decreases to ~25 μm after 500 μm. The final plastic zone region for Zr-BMG with T_f = 683 K with 0 cycle was observed to be 430 μm, then lowered to ~260 at 200 cycles, and then increases to 485 μm after 700 cycles. Zr-BMG with T_f = 603 K without thermal cycling shows R_p of 175 μm, while the same condition after 200 cycles shows a similar R_p of 165 μm. For all conditions, the plastic zone size before fracture scales

with the measured fracture toughness and exhibit the same overall trend with the measured fracture toughness.

We applied an analysis introduced by Narayan et. al. which connects shear band density and fracture toughness in BMGs through $K_Q = 16.95(N_n)^{0.5}$ [39]. Measured K_Q is plotted against the corresponding number of shear band ahead of the notch tip (Fig. 3(c)). Our analysis reveals that above correlation, which has been widely confirmed for BMGs in their as-cast and annealed states also persists in thermally cycled samples.

To gain further insights into the effect of thermal cycling on fracture toughness we evaluated representative fracture surfaces of the fracture toughness samples (Figure 3(b)). Pd-BMG exhibits the characteristic vein pattern over the fracture surface. For Pd-BMG with T_f = 633 K cycled for 200 cycles (K_Q = 56±5 MPa·m$^{1/2}$), a rougher surface is present compare to 0 cycles (K_Q = 38.0 ± 1.0 MPa m$^{1/2}$) and 300 cycles (K_Q = 39 ± 5 MPa·m$^{1/2}$). Pd-BMG with T_f = 573 K which was cycled for 50 times (K_Q = 12.1 ± 0.3 MPa m$^{1/2}$) shows a noticeably smoother surface compared to the 0 cycle (K_Q = 25.0 ± 6.0 MPa m$^{1/2}$) and 200 cycle (K_Q = 22.0 ± 1.0 MPa m$^{1/2}$) samples. This trend of fracture surface roughness supports the K_Q data as rough fracture surfaces are associated with ductile fracture and a smooth surface is associated with brittle behavior [44-46]. This is also the case for the Zr-BMGs where riverlike patterns dominate the surface of Zr-BMG with T_f = 683 K, suggesting a ductile fracture. Zr-BMG with T_f = 683 K cycled 200 times (K_Q = 57.76 ± 12.9 MPa m$^{1/2}$) show a slightly smoother surface compared glasses at 0 cycle and cycled 700 times. For Zr-BMG with T_f = 603 K at 0 cycle and 200 cycles both shows similar vein-like pattern behavior.

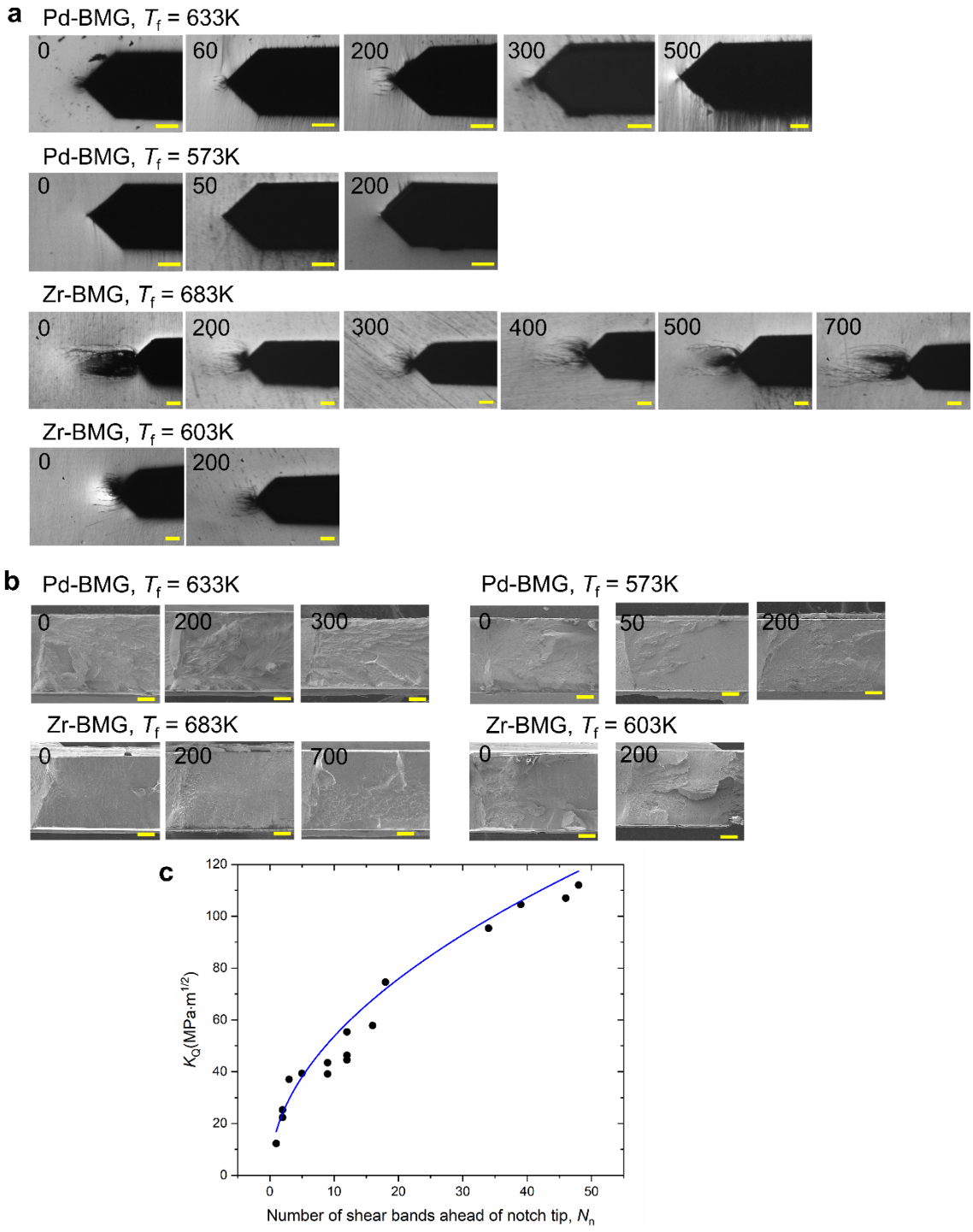

Figure 3 Plastic zone region and fracture surface analysis of the fracture toughness samples. (a) Plastic zone region ahead of the notch tip before fracture for Pd-BMG with T_f = 633 K, Pd-BMG with T_f = 573 K, Zr-BMG with T_f = 683 K, Zr-BMG with T_f = 603 K from top to bottom. All scale bars are 100 μm. (b) Fractography of fracture toughness samples after fractured for Pd-BMG and Zr-BMG at various fictive temperatures and various thermal cycles. All scale bars are 50 μm. (c) Relationship between fracture toughness, K_Q, and number of shear bands ahead of notch tip Nn,

collected in this experiment as shown in (a). Blue curve represents $K_Q = 16.95(N_n)^{0.5}$ for the experimentally determined *N*n [39].

In order to evaluate the effect of the magnitude of the thermal cycling, we considered a different cycling temperature range (amplitude). Specifically, we cycled between 195 K and room temperature (298 K) with acetone/dry ice bath, giving a temperature variation of 103 K. For all experiments the effect of 103 K cycling was unnoticeable after 50 cycles. Only for Pd-BMG with T_f = 633 K, a subtle increase from 38 ± 1 MPa·m$^{1/2}$ to 41± 1 MPa·m$^{1/2}$ after 50 cycles was observed.

3.2 The effect of thermal cycling on the glasses' structures and thermal properties

Thermal analysis and high energy X-ray experiments were carried out to gain insight on the microscopic origin, resulting in the thermal cycling induced K_Q changes, and corresponding rejuvenation or relaxation processes (Fig. 4 and 5). Within our thermal analysis, no obvious trend connecting heat capacity with K_Q that is consistent among all considered alloys is present. It has been suggested that rejuvenated BMGs, exhibit a drop of heat capacity prior to T_g quantified in the heat of relaxation, ΔH_{rel} [16]. Fig. 4(a)-(d) shows the heat capacity of Pd-BMG with T_f = 573 K, Pd-BMG with T_f = 633 K, Zr-BMG with T_f = 633 K and as-cast La-BMG, respectively. K_Q data on La-BMG could not be determined as the material is too brittle for a reliable measurement. Fig. 4(e) summarizes the heat of relaxation as measured from the DSC for the studied BMGs. For the considered BMGs, ΔH_{rel} and mechanical response, K_Q do not follow the expected correlation, namely that ΔH_{rel} and K_Q are proportional. It is important to mention that the changes in c_p are very small, comparable to the experimental resolution of DSC, and approximately 1/50 of a crystallization signal. Such difficulty to precisely determine ΔH_{rel} may also reflect in the wide range of previous results [16, 21, 41]. Some previous studies on thermal cycling of MGs have reported a consistent trend, improvement in ductility and increase in ΔH_{rel} [16], whereas in other

studies the correlation is unclear and the authors suggested that the inconsistency might originate from the weak thermal signal [21, 41]. Such a weak correlation between thermal signal and mechanical properties with thermal cycling may also suggest that the origins of structural changes affecting mechanical properties may not entirely be the same than those affecting the thermal behavior. For this argument, one has to keep in mind that thermodynamics properties reflect average changes that usually originate from affine structural changes. Most of the mechanical properties involving plasticity are predominantly affected by non-affine contributions [29, 47-51].

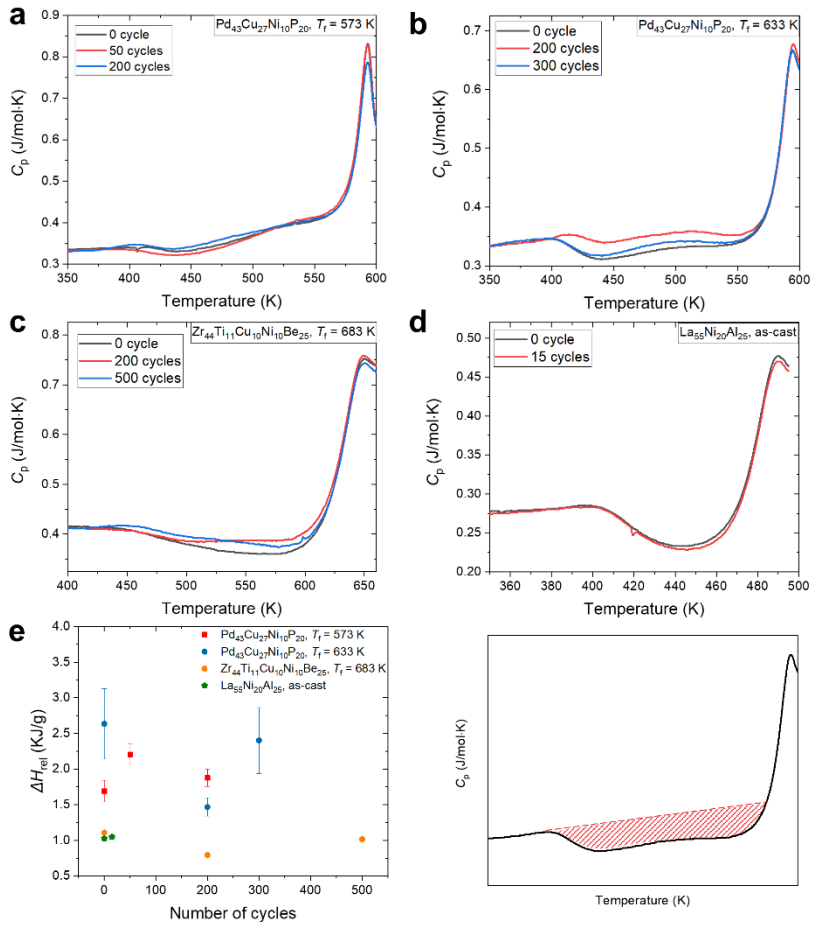

Figure 4. Thermogram of thermally cycled (a) Pd-BMG with original T_f of 573K, (b) Pd-BMG with original T_f of 633 K, (c) Zr-BMG with original T_f of 683K and (d) as-cast La-BMG and (e) heat of relaxation versus number of cycles for the studied alloys (left), the heat of relaxation is measured by the shaded area.

In order to directly measure the effect of thermal cycling on the structure of the various BMGs, we utilized high energy X-ray diffraction (Fig. 5). The pair distribution function, $\rho(r)$, shows that structural changes which originate from thermal cycling follow trends and correlate with the measured K_Q. For example, the Pd-BMG with T_f = 573K increases its packing density, which can be concluded from the peak height of the first peak, which is increasing after 50 cycles. With further cycling to 200 cycles, the packing density decreases towards the direction of the original value (Fig 5(a)). This behavior is consistent with the behavior of the corresponding K_Q behavior and is in line with the current understanding of structure-property relationships in BMGs which suggests densely packed glasses generally behave in a brittle manner [52-54]. Similarly, Pd-BMG with T_f = 633K which becomes less densely packed after 200 cycles experience an increase in K_Q (Fig. 5(b)). Zr-BMG with T_f = 683 K becomes more densely packed after 200 cycles, which correlates with a decrease in K_Q at 200 cycles. At 700 cycles ρ(r) is reduced compare to 200 cycles, indicating of a reversal in the packing trend to a more loosely packed structure (Fig. 5(d)).

Comparing the dependence of thermal cycling on the K_Q and $\rho(r)$ suggests a correlation between $\rho(r)$ and K_Q. Figure 5 (a) shows that for Pd-BMG with T_f = 573 K, glasses that have been cycled for 50 times are the most densely packed, followed by 200 cycles, then 0 cycle. This corresponds to the observed minimum K_Q subjected to 50 cycles of thermal cycling. The same is true for Pd-BMG with T_f = 633 K (Fig. 5(b)), where glasses cycled for 200 cycles exhibit the most loosely packed structure, which coincides with the maximum K_Q, observed in this system and T_f condition. All of the above cases studied and discussed are summarized in Fig. 5(e). Figure 5 (c) and (d) shows that Zr-BMGs with T_f = 593 K and T_f = 683 cycled for 200 times exhibit a denser packed structure compared to the original T_f state before cycling, also coincides well with the decrease in

K_Q due to thermal cycling. It is important to emphasize that even though the PDF follows the trends of the K_Qs, they are not identical where the K_Qs are identical. For example, the K_Q of Pd-BMG with T_f = 633 K pre-cycled and after 300 cycles shares identical K_Qs at ~ 39 MPa·m$^{1/2}$ (within experimental error) but the PDFs are not. This means that different structures can result in identical mechanical responses. If that would not be the case, further cycling would result in another rejuvenation or relaxation cycle. Such oscillations do not occur, see for example Pd-BMG T_f = 633 K (Fig.2a) and Zr-BMG T_f = 683 K (Fig 2b).

To better visualize the correlation between the effect of the various thermal cycling procedures on the structure of each alloy, we summarize the observation by plotting the maximum value of ρ(r), $\rho(r)_{maximum}$, against the number of cycles for each alloy and T_f (Fig.4 (e)). Such plot reveals that the original and final states prior and post-thermal cycling have similar $\rho(r)_{maximum}$, while the states in between have a higher $\rho(r)_{maximum}$ when the measured K_Q is lower than the original value (and a lower $\rho(r)_{maximum}$ when measured K_Q is higher than the original value). It is important to restate that ρ(r) is an average measure. As we anticipate, and recent studies provided more evidence [20, 55], thermal cycling predominantly causes non-affine structural changes. Even though the effect of thermal cycling on these non-affine regions, often referred to as soft spots or shear transformation zones precursors, might be very large, due to their small volume fraction, the effect on ρ(r) is small but consistent.

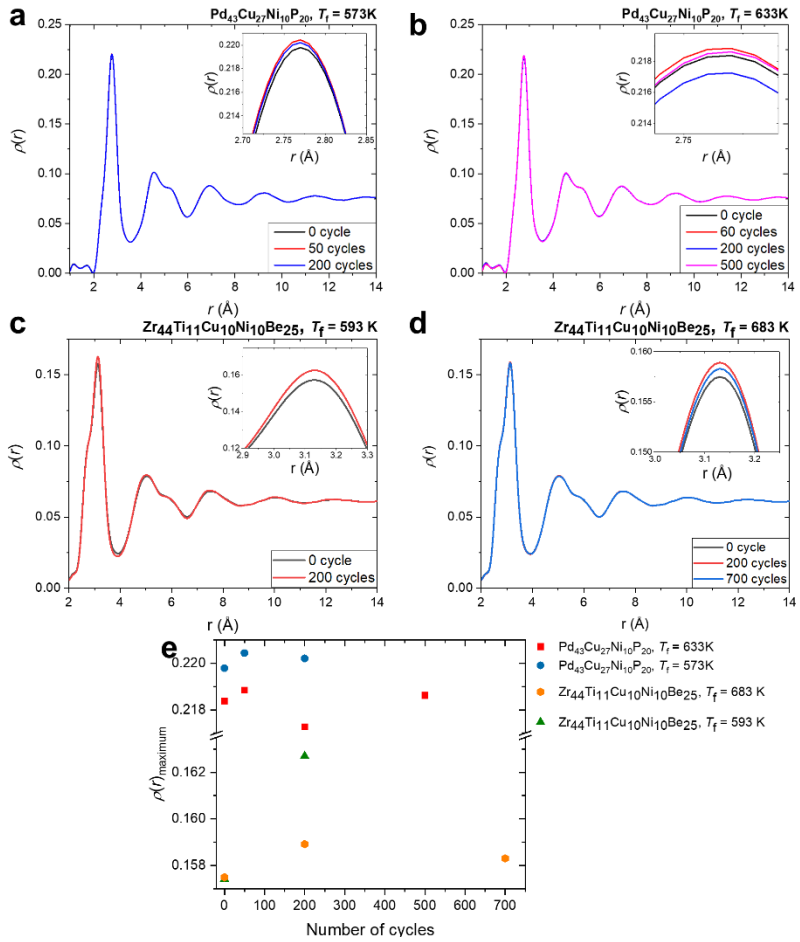

Figure 5. Pair distribution function of (a) $Pd_{43}Cu_{27}Ni_{10}P_{20}$ T_f = 573 K, (b) $Pd_{43}Cu_{27}Ni_{10}P_{20}$ T_f = 633 K, (c) $Zr_{44}Ti_{11}Cu_{10}Ni_{10}Be_{25}$ T_f = 593 K, (d) $Zr_{44}Ti_{11}Cu_{10}Ni_{10}Be_{25}$ T_f = 683 K and (e) summarizes the maximum of the pair distribution function, $\rho(r)_{maximum}$, for studied alloys and T_f's.

However, even though a clear correlation between atomic structure and mechanical properties and their dependence of thermal cycling is revealed here, the richness of behaviors, reflecting in even qualitatively different responses of thermal cycling on mechanical properties (K_Q) and structural changes (reflected in $\rho(r)$), is surprising. Previous mechanistic microscopic explanations of the microscopic origins responsible for property changes during thermal cycling suggest monotonic but continuously decreasing rejuvenation [16, 20, 56]. The exception is a recent molecular dynamics study, which reported that low energy states (low T_f) respond to thermal cycling by increasing their energy (rejuvenate), whereas high energy states (high T_f) decrease their energy

during thermal cycling [55]. In previous experimental studies, it has been suggested that local stresses which themselves originate from local variation in thermal expansion coefficient cause rejuvenation during thermal cycling [16, 21, 57]. As local variation in thermal expansion coefficient would continuously decrease with thermal cycling, such a mechanism cannot explain the observed non-monotonic behavior which we have revealed here for both cases, with an initial increase or decrease in K_Q. Our results suggest that the effect of thermal cycling on the structure and properties of BMGs is determined by multiple influences and their relative contributions determine the behavior of K_Q and $\rho(r)_{maximum}$. Such contribution may potentially be the previously suggested local variation in thermal expansion coefficient which can be considered as the amplitude of the excitation during thermal cycling, E [16, 57]. E is envisioned to be initially large in highly heterogenous structures and continuously decrease with thermal cycling as the structure becomes more homogeneous [58]. This is due to the fact that as the local stresses homogenize, the structure where regions of low thermal expansion coefficient increase in density and vice versa. Such homogenization would result in a monotonic decrease of E with increasing cycle number.

The non-monotonic behavior and the qualitatively different effects of thermal cycling on fracture toughness of BMGs suggest that E has to be compete and compared with other quantities, where these quantities vary in glasses of different structural state and chemistry. As the structure measurements (Fig.5) suggest structural changes due to thermal cycling, associated contributions of thermal cycling suggest involving rearrangements. Such rearrangements, which can occur at stress levels significantly below the yield strength [59-65] can be microscopically associated with α-relaxation processes [66]. As the α-relaxation processes are defined by an activation barrier to evolve from one structural state to another, it is reasonable to assume that such barriers and their relative magnitude compare to E play a role in the fracture toughness response to the thermal

cycling of metallic glasses. As these activation energies and the density of states change significantly with potential energy, (and thus, T_f) and thereby through thermal cycling their value and E, it is difficult to suggest an analytical description. For example, whether a glass structure will increase or decrease in potential energy through thermal cycling will depend on the relative quantities of E and activation energies, which are both unknown and undergo constant changes during cycling. It should also be mentioned that even though overall a net increase or decrease in potential energy is observed, both processes, rejuvenation and relaxation may occur simultaneously. However, depending on the conditions, their occurrence may be different in quantity and location within the glass.

Conclusion:

For a wider range of BMGs in various structural states, we studied the effect of thermal cycling on structure, thermal signal, and fracture toughness. Oppose to previously reported monotonic rejuvenation as an effect of thermal cycling, we revealed a wide range of behaviors, including non-monotonic rejuvenation and relaxation. With increasing cycle number, fracture toughness increases or decreases, goes through a minimum or maximum, and with further cycling decreases or increase back towards a metastable equilibrium value. Such richness in behaviors suggest that the previous picture of monotonically decreasing local stresses resulting in a homogenization of the structure with increasing cycle is incomplete. Our finding suggests that relative comparisons of various contributions which are also constantly changing decide if further cycling results in an increase or decrease in fracture toughness. The effects of cycling on fracture toughness can be correlated with structural changes of the glass but not obviously with a thermal signature.

Acknowledgement

The authors thank Prof. Eran Bouchbinder and Prof. Lindsay Greer for insightful discussions. Experimental assistance from Zengquan Wang is gratefully acknowledged. This work was supported by the U.S. Department of Energy through the Office of Science, Basic Energy Science, Materials Science and Engineering Division (No. DE SC0004889).

References:

[1] A.Q. Tool, RELATION BETWEEN INELASTIC DEFORMABILITY AND THERMAL EXPANSION OF GLASS IN ITS ANNEALING RANGE*, Journal of the American Ceramic Society 29(9) (1946) 240-253.
[2] O.S. NARAYANASWAMY, A Model of Structural Relaxation in Glass, Journal of the American Ceramic Society 54(10) (1971) 491-498.
[3] V.H. Hammond, M.D. Houtz, J.M. O'Reilly, Structural relaxation in a bulk metallic glass, Journal of Non-Crystalline Solids 325(1) (2003) 179-186.
[4] G. Kumar, D. Rector, R.D. Conner, J. Schroers, Embrittlement of Zr-based bulk metallic glasses, Acta Materialia 57(12) (2009) 3572-3583.
[5] P. Murali, U. Ramamurty, Embrittlement of a bulk metallic glass due to sub-Tg annealing, Acta Materialia 53(5) (2005) 1467-1478.
[6] J. Carter, E.G. Fu, G. Bassiri, B.M. Dvorak, N. David Theodore, G. Xie, D.A. Lucca, M. Martin, M. Hollander, X. Zhang, L. Shao, Effects of ion irradiation in metallic glasses, Nuclear Instruments and Methods in Physics Research Section B: Beam Interactions with Materials and Atoms 267(8) (2009) 1518-1521.
[7] E.A. Kramer, W.L. Johnson, C. Cline, The effects of neutron irradiation on a superconducting metallic glass, Applied Physics Letters 35(10) (1979) 815-818.
[8] D.J. Magagnosc, G. Kumar, J. Schroers, P. Felfer, J.M. Cairney, D.S. Gianola, Effect of ion irradiation on tensile ductility, strength and fictive temperature in metallic glass nanowires, Acta Materialia 74 (2014) 165-182.
[9] S.G. Mayr, Impact of ion irradiation on the thermal, structural, and mechanical properties of metallic glasses, Physical Review B 71(14) (2005) 144109.
[10] A.R. Yavari, K. Georgarakis, W.J. Botta, A. Inoue, G. Vaughan, Homogenization of plastic deformation in metallic glass foils less than one micrometer thick, Physical Review B 82(17) (2010) 172202.
[11] X.D. Wang, Q.P. Cao, J.Z. Jiang, H. Franz, J. Schroers, R.Z. Valiev, Y. Ivanisenko, H. Gleiter, H.J. Fecht, Atomic-level structural modifications induced by severe plastic shear deformation in bulk metallic glasses, Scripta Materialia 64(1) (2011) 81-84.
[12] S. Scudino, B. Jerliu, K.B. Surreddi, U. Kühn, J. Eckert, Effect of cold rolling on compressive and tensile mechanical properties of Zr52.5Ti5Cu18Ni14.5Al10 bulk metallic glass, Journal of Alloys and Compounds 509 (2011) S128-S130.

[13] M. Zhang, Y.M. Wang, F.X. Li, S.Q. Jiang, M.Z. Li, L. Liu, Mechanical Relaxation-to-Rejuvenation Transition in a Zr-based Bulk Metallic Glass, Scientific Reports 7(1) (2017) 625.
[14] M. Samavatian, R. Gholamipour, A.A. Amadeh, S. Mirdamadi, Extra rejuvenation of Zr55Cu30Al10Ni5 bulk metallic glass using elastostatic loading and cryothermal treatment interaction, Journal of Non-Crystalline Solids 506 (2019) 39-45.
[15] W. Guo, R. Yamada, J. Saida, S. Lü, S. Wu, Thermal rejuvenation of a heterogeneous metallic glass, Journal of Non-Crystalline Solids 498 (2018) 8-13.
[16] S.V. Ketov, Y.H. Sun, S. Nachum, Z. Lu, A. Checchi, A.R. Beraldin, H.Y. Bai, W.H. Wang, D.V. Louzguine-Luzgin, M.A. Carpenter, A.L. Greer, Rejuvenation of metallic glasses by non-affine thermal strain, Nature 524(7564) (2015) 200-3.
[17] W. Guo, R. Yamada, J. Saida, Rejuvenation and plasticization of metallic glass by deep cryogenic cycling treatment, Intermetallics 93 (2018) 141-147.
[18] X.L. Bian, G. Wang, J. Yi, Y.D. Jia, J. Bednarčík, Q.J. Zhai, I. Kaban, B. Sarac, M. Mühlbacher, F. Spieckermann, J. Keckes, J. Eckert, Atomic origin for rejuvenation of a Zr-based metallic glass at cryogenic temperature, Journal of Alloys and Compounds 718 (2017) 254-259.
[19] R. Myong-Chol, S. Sajad, D. Da-Wei, D. Bang-Shao, Z. Shao-Xiong, W. Wei-Hua, Serrated magnetic properties in metallic glass by thermal cycle, Chinese Physics B 26(6) (2017) 066101.
[20] T.J. Lei, L.R. DaCosta, M. Liu, W.H. Wang, Y.H. Sun, A.L. Greer, M. Atzmon, Microscopic characterization of structural relaxation and cryogenic rejuvenation in metallic glasses, Acta Mater 164 (2019) 165-170.
[21] W. Song, X. Meng, Y. Wu, D. Cao, H. Wang, X. Liu, X. Wang, Z. Lu, Improving plasticity of the Zr46Cu46Al8 bulk metallic glass via thermal rejuvenation, Science Bulletin 63(13) (2018) 840-844.
[22] X. Bian, G. Wang, Q. Wang, B. Sun, I. Hussain, Q. Zhai, N. Mattern, J. Bednarčík, J. Eckert, Cryogenic-temperature-induced structural transformation of a metallic glass, Materials Research Letters 5(4) (2017) 284-291.
[23] H. Zheng, L. Zhu, S.S. Jiang, Y.G. Wang, F.G. Chen, Recovering the bending ductility of the stress-relieved Fe-based amorphous alloy ribbons by cryogenic thermal cycling, Journal of Alloys and Compounds 790 (2019) 529-535.
[24] C.J. Gilbert, R.O. Ritchie, W.L. Johnson, Fracture toughness and fatigue-crack propagation in a Zr–Ti–Ni–Cu–Be bulk metallic glass, Applied Physics Letters 71(4) (1997) 476.
[25] J. Ketkaew, W. Chen, H. Wang, A. Datye, M. Fan, G. Pereira, U.D. Schwarz, Z. Liu, R. Yamada, W. Dmowski, M.D. Shattuck, C.S. O'Hern, T. Egami, E. Bouchbinder, J. Schroers, Mechanical glass transition revealed by the fracture toughness of metallic glasses, Nature communications 9(1) (2018) 3271.
[26] G.R. Garrett, M.D. Demetriou, M.E. Launey, W.L. Johnson, Origin of embrittlement in metallic glasses, Proceedings of the National Academy of Sciences 113(37) (2016) 10257.
[27] C.A. Schuh, T.C. Hufnagel, U. Ramamurty, Overview No.144 - Mechanical behavior of amorphous alloys, Acta Mater 55(12) (2007) 4067-4109.
[28] I. Gallino, J. Schroers, R. Busch, Kinetic and thermodynamic studies of the fragility of bulk metallic glass forming liquids, J Appl Phys 108(6) (2010).
[29] J. Ketkaew, W. Chen, H. Wang, A. Datye, M. Fan, G. Pereira, U.D. Schwarz, Z. Liu, R. Yamada, W. Dmowski, M.D. Shattuck, C.S. O'Hern, T. Egami, E. Bouchbinder, J. Schroers, Mechanical glass transition revealed by the fracture toughness of metallic glasses, Nature Communications 9 (2018).

[30] A.J. Kailath, A. Kumar, A. Mitra, Effect of metalloids on crystallization and magnetic behaviour of FeCoSiB based metallic glass, Bulletin of Materials Science 29(2) (2006) 127-131.
[31] G. Kumar, S. Prades-Rodel, A. Blatter, J. Schroers, Unusual brittle behavior of Pd-based bulk metallic glass, Scripta Mater 65(7) (2011) 585-587.
[32] B. Sarac, J. Ketkaew, D.O. Popnoe, J. Schroers, Honeycomb Structures of Bulk Metallic Glasses, Advanced Functional Materials 22(15) (2012) 3161-3169.
[33] W. Chen, J. Ketkaew, Z. Liu, R.M.O. Mota, K. O'Brien, C.S. da Silva, J. Schroers, Does the fracture toughness of bulk metallic glasses scatter?, Scripta Materialia 107 (2015) 1-4.
[34] W. Chen, H.F. Zhou, Z. Liu, J. Ketkaew, L. Shao, N. Li, P. Gong, W. Samela, H.J. Gao, J. Schroers, Test sample geometry for fracture toughness measurements of bulk metallic glasses, Acta Mater 145 (2018) 477-487.
[35] W. Chen, Z. Liu, J. Ketkaew, R.M.O. Mota, S.H. Kim, M. Power, W. Samela, J. Schroers, Flaw tolerance of metallic glasses, Acta Materialia 107 (2016) 220-228.
[36] H. Vogel, The temperature dependence law of the viscosity off luids, PHYSIKALISCHE ZEITSCHRIFT 22 (1921) 645-646.
[37] S. Fulcher Gordon, ANALYSIS OF RECENT MEASUREMENTS OF THE VISCOSITY OF GLASSES, Journal of the American Ceramic Society 8(6) (1925) 339-355.
[38] W. Chen, J. Ketkaew, Z. Liu, R.M.O. Mota, K. O'Brien, C.S. da Silva, J. Schroers, Does the fracture toughness of bulk metallic glasses scatter?, Scripta Materialia 107 (2015) 1-4.
[39] R.L. Narayan, D. Raut, U. Ramamurty, A quantitative connection between shear band mediated plasticity and fracture initiation toughness of metallic glasses, Acta Materialia 150 (2018) 69-77.
[40] A.P. Hammersley, S.O. Svensson, A. Thompson, Calibration and correction of spatial distortions in 2D detector systems, Nuclear Instruments and Methods in Physics Research Section A: Accelerators, Spectrometers, Detectors and Associated Equipment 346(1) (1994) 312-321.
[41] X. Wang, Y. Shao, P. Gong, K.F. Yao, The effect of simulated thermal cycling on thermal and mechanical stability of a Ti-based bulk metallic glass, Journal of Alloys and Compounds 575 (2013) 449-454.
[42] T.C. Hufnagel, U.K. Vempati, J.D. Almer, Crack-Tip Strain Field Mapping and the Toughness of Metallic Glasses, PLOS ONE 8(12) (2013) e83289.
[43] S. Scudino, R.N. Shahid, B. Escher, M. Stoica, B.S. Li, J.J. Kruzic, Mapping the cyclic plastic zone to elucidate the mechanisms of crack tip deformation in bulk metallic glasses, Applied Physics Letters 110(8) (2017) 081903.
[44] X.K. Xi, D.Q. Zhao, M.X. Pan, W.H. Wang, Y. Wu, J.J. Lewandowski, Fracture of brittle metallic glasses_ brittleness or plasticity, Physical Review Letters 94 (2005) 125510.
[45] C.J. Gilbert, V. Schroeder, R.O. Ritchie, Mechanisms for fracture and fatigue-crack propagation in a bulk metallic glass, Metall and Mat Trans A 30(7) (1999) 1739-1753.
[46] G. Wang, Y.T. Wang, Y.H. Liu, M.X. Pan, D.Q. Zhao, W.H. Wang, Evolution of nanoscale morphology on fracture surface of brittle metallic glass, Applied Physics Letters 89(12) (2006) 121909.
[47] M. Vasoya, C.H. Rycroft, E. Bouchbinder, Notch Fracture Toughness of Glasses: Dependence on Rate, Age, and Geometry, Phys Rev Appl 6(2) (2016).
[48] T.W. Wu, F. Spaepen, The Relation between Embrittlement and Structural Relaxation of an Amorphous Metal, Philosophical Magazine B-Physics of Condensed Matter Statistical Mechanics Electronic Optical and Magnetic Properties 61(4) (1990) 739-750.

[49] J. Ashwin, E. Bouchbinder, I. Procaccia, Cooling-rate dependence of the shear modulus of amorphous solids, Phys Rev E 87(4) (2013).
[50] G.R. Garrett, M.D. Demetriou, M.E. Launey, W.L. Johnson, Origin of embrittlement in metallic glasses, P Natl Acad Sci USA 113(37) (2016) 10257-10262.
[51] J. Ketkaew, M. Fan, M.D. Shattuck, C.S. O'Hern, J. Schroers, Structural relaxation kinetics defines embrittlement in metallic glasses, Scripta Mater 149 (2018) 21-25.
[52] J. Schroers, W.L. Johnson, Ductile bulk metallic glass, Phys Rev Lett 93(25) (2004).
[53] C.H. Rycroft, E. Bouchbinder, Fracture Toughness of Metallic Glasses: Annealing-Induced Embrittlement, Phys Rev Lett 109(19) (2012).
[54] Y.Q. Cheng, H.W. Sheng, E. Ma, Relationship between structure, dynamics, and mechanical properties in metallic glass-forming alloys, Phys Rev B 78(1) (2008) -.
[55] N.V. Priezjev, The effect of cryogenic thermal cycling on aging, rejuvenation, and mechanical properties of metallic glasses, J Non-Cryst Solids 503 (2019) 131-138.
[56] J. Pan, Y.X. Wang, Q. Guo, D. Zhang, A.L. Greer, Y. Li, Extreme rejuvenation and softening in a bulk metallic glass, Nature Communications 9 (2018).
[57] T.C. Hufnagel, Cryogenic rejuvenation, Nature materials 14 (2015) 867.
[58] T.C. Hufnagel, METALLIC GLASSES Cryogenic rejuvenation, Nat Mater 14(9) (2015) 867-868.
[59] J.D. Ju, D. Jang, A. Nwankpa, M. Atzmon, An atomically quantized hierarchy of shear transformation zones in a metallic glass, J Appl Phys 109(5) (2011).
[60] F. Spaepen, Creep, Viscosity and Structural Relaxation in Metallic Glasses, Jom-J Min Met Mat S 32(8) (1980) 23-23.
[61] I. Regev, J. Weber, C. Reichhardt, K.A. Dahmen, T. Lookman, Reversibility and criticality in amorphous solids, Nature Communications 6 (2015).
[62] Y. Fan, T. Iwashita, T. Egami, How thermally activated deformation starts in metallic glass, Nature Communications 5 (2014).
[63] M. Fan, K. Zhang, J. Schroers, M.D. Shattuck, C.S. O'Hern, Particle rearrangement and softening contributions to the nonlinear mechanical response of glasses, Phys Rev E 96(3) (2017).
[64] M. Kanik, P. Bordeenithikasem, G. Kumar, E. Kinser, J. Schroers, High quality factor metallic glass cantilevers with tunable mechanical properties, Appl Phys Lett 105(13) (2014).
[65] M. Kanik, P. Bordeenithikasem, D. Kim, N. Selden, A. Desai, R. M'Closkey, J. Schroers, Metallic Glass Hemispherical Shell Resonators, J Microelectromech S 24(1) (2015) 19-28.
[66] S. Sastry, P.G. Debenedetti, F.H. Stillinger, Signatures of distinct dynamical regimes in the energy landscape of a glass-forming liquid, Nature 393(6685) (1998) 554-557.